SOIL RESPIRATION

Soil respiration–driven CO$_2$ pulses dominate Australia's flux variability

Eva-Marie Metz[1]*, Sanam N. Vardag[1,2], Sourish Basu[3,4], Martin Jung[5], Bernhard Ahrens[5], Tarek El-Madany[5], Stephen Sitch[6], Vivek K. Arora[7], Peter R. Briggs[8], Pierre Friedlingstein[9,10], Daniel S. Goll[11], Atul K. Jain[12], Etsushi Kato[13], Danica Lombardozzi[14], Julia E. M. S. Nabel[5,15], Benjamin Poulter[16], Roland Séférian[17], Hanqin Tian[18], Andrew Wiltshire[19], Wenping Yuan[20], Xu Yue[21], Sönke Zaehle[5], Nicholas M. Deutscher[22], David W. T. Griffith[22], André Butz[1,2,23]*

The Australian continent contributes substantially to the year-to-year variability of the global terrestrial carbon dioxide (CO$_2$) sink. However, the scarcity of in situ observations in remote areas prevents the deciphering of processes that force the CO$_2$ flux variability. In this study, by examining atmospheric CO$_2$ measurements from satellites in the period 2009–2018, we find recurrent end-of-dry-season CO$_2$ pulses over the Australian continent. These pulses largely control the year-to-year variability of Australia's CO$_2$ balance. They cause two to three times larger seasonal variations compared with previous top-down inversions and bottom-up estimates. The pulses occur shortly after the onset of rainfall and are driven by enhanced soil respiration preceding photosynthetic uptake in Australia's semiarid regions. The suggested continental-scale relevance of soil-rewetting processes has substantial implications for our understanding and modeling of global climate–carbon cycle feedbacks.

Terrestrial ecosystems drive the seasonal and year-to-year variability of the global carbon dioxide (CO$_2$) sink (1). Previous research has identified semiarid regions as hotspots of global CO$_2$ balance interannual variability (2–5) because of the strong sensitivity of photosynthetic carbon uptake to fluctuations in water availability (6, 7). The Australian continent is primarily covered with semiarid ecosystems and experiences large variations in rainfall. These conditions make Australia particularly relevant for the variability in the global carbon cycle (8–13), contributing up to 60% of yearly anomalies in the global terrestrial CO$_2$ sink (2).

However, attribution of global CO$_2$ sink variations to certain regions and mechanisms is highly uncertain, which limits our ability to model climate–carbon cycle feedbacks and project future climate (14, 15). Global process-based ecosystem models underestimate observed CO$_2$ flux variability across semiarid sites owing to the complexity of carbon–water cycle interactions and the diversity of ecosystem responses to water fluctuations (16, 17). The same holds true for machine learning–based models trained on local carbon flux observations (18, 19) given the scarcity of available

flux measurements in low-latitude semiarid regions (20) and the inability to represent potentially important noninstantaneous carry-over effects (21). Atmospheric transport inversions based on in situ measurements of airborne CO$_2$ also suffer from the scarcity of observations in remote areas, and therefore the inversions cannot reliably attribute CO$_2$ flux variability to specific regions, despite growing monitoring capacities (22, 23). However, recent satellite observations of atmospheric column CO$_2$ deliver data where ground-based in situ concentration measurements and carbon flux networks are sparse, and thus, satellite CO$_2$ data can fill important gaps and provide new constraints on regional-scale patterns and processes (8, 24–28).

In this study, using satellite observations of atmospheric CO$_2$ concentrations from the Greenhouse Gases Observing Satellite (GOSAT) for the period 2009–2018, we identify a net CO$_2$ pulse to the atmosphere of variable magnitude that occurs over Australia at the end of the dry season in most years. We show that this pattern—which is not evident in traditional atmospheric inversions using in situ measurements only, in the FLUXCOM machine learning–based extrapolations of in situ flux measurements (18, 20), or in most process-

based ecosystem models of the TRENDY initiative (29)—appears to dominate the seasonal and year-to-year variations of Australia's CO$_2$ balance for that period. The few process-based TRENDY models that reproduce the CO$_2$ pulse pattern qualitatively suggest that it is caused by rapid respiratory carbon release with the onset of the rainy season while the increase in photosynthetic carbon uptake lags behind. This observed process is consistent with the phenomenon of respiration pulses after rewetting events discussed in the context of the "Birch effect" (30, 31). Such pulses have been described extensively in local studies of water-limited systems (32), but their large-scale relevance has remained unknown.

Atmospheric CO$_2$ peak over Australia

The GOSAT has been delivering global measurements of the column-average dry-air mole fractions ("concentrations") of atmospheric CO$_2$ since its launch in 2009 (33). After subtracting the secular trend (34), the record of GOSAT concentrations for the period 2009–2018 (Fig. 1) reveals a seasonal pattern above Australia with CO$_2$ drawdown in March, April, and May (MAM) and a CO$_2$ peak of variable magnitude at the end of the dry season in October, November, and December (OND). These patterns are consistent among two retrievals independently applied to GOSAT [GOSAT/RemoTeC (35) and GOSAT/ACOS (36); table S1], and they are present in CO$_2$ concentrations measured by the Orbiting Carbon Observatory-2 [OCO-2 (37, 38), period 2015–2018; table S1) as well as in ground-based data of the Total Carbon Column Observing Network (TCCON) (39) (figs. S1 and S2).

In contrast, the atmospheric column CO$_2$ concentrations simulated by three inverse atmospheric transport models—CarbonTracker CT2019B (40), CAMS (41), and TM5-4DVAR (42)—underestimate the CO$_2$ drawdown in MAM and lack the CO$_2$ pulses in OND (Fig. 1). Driven by atmospheric wind data, these transport models deliver concentration fields that are optimally compatible with in situ–measured CO$_2$ concentrations and the a priori biogenic, oceanic, fire, and fossil CO$_2$ surface-atmosphere fluxes (34). However, given their sparsity in

and around Australia (compare fig. S3 and fig. S4), the in situ measurements provide only marginal constraints on the regional flux balance. Thus, the discrepancy between CO_2 concentrations from GOSAT and traditional in situ–based atmospheric inversions hints at the existence of a carbon release mechanism in Australian ecosystems that has remained undetected by the existing in situ CO_2 monitoring system.

Australian top-down and bottom-up fluxes

To improve upon the surface flux estimates for Australia, we fed the GOSAT CO_2 concentrations into one of the atmospheric inverse models (TM5-4DVAR) together with the in situ CO_2 measurements. We find that the recurring end-of-dry-season CO_2 concentration peaks are indeed attributed to a carbon release pattern originating from land ecosystems, which is not present in the inversions when assimilating in situ CO_2 data alone (Fig. 2A and fig. S5).

Our new estimates of Australia's carbon balance variability based on assimilating GOSAT together with in situ data show a nearly doubled peak-to-peak amplitude of the seasonal cycle (175 ± 40 TgC/month, mean ± standard deviation over the 2009–2018 period, July-to-June peak-to-peak amplitude) compared with the in situ–only inversions (88 ± 13 TgC/month). Moreover, the end-of-dry-season CO_2 pulses found by the GOSAT inversions imply a more than fourfold greater year-to-year variability of the annual CO_2 fluxes (0.207 PgC/year, standard deviation over the 2010–2018 period) than for the in situ–only inversions (0.039 PgC/year) (fig. S6 and table S2). Fluxes obtained by assimilating OCO-2 together with in situ data for the period 2015–2018 show the same end-of-dry-season pulses and agree well with the fluxes of the GOSAT inversion (fig. S7).

To understand the origin of the CO_2 pulses, we compared the top-down inversions with bottom-up estimates from machine learning [FLUXCOM (18, 20)] and 18 process-based dynamic global vegetation models (DGVMs) from the TRENDY (v9) ensemble (42). The DGVMs also provide the component fluxes of gross primary productivity (GPP) and terrestrial ecosystem respiration (TER) enabling the attribution to variations in photosynthetic carbon uptake and respiratory carbon release. We further included fire emissions (FIRE) from the Global Fire Emission Database (GFED) as a potential factor for explaining the pattern. To compare with the top-down inversions, we calculated net biome production (NBP = TER + FIRE – GPP) by adding fire emissions from GFED to net ecosystem exchange (NEE = TER – GPP) from FLUXCOM. With this sign convention, positive fluxes correspond to carbon emissions into the atmosphere. For TRENDY, NBP was taken directly from the simulations of the DGVMs. We find that FLUXCOM+GFED–derived NBP lacks the end-of-dry-season
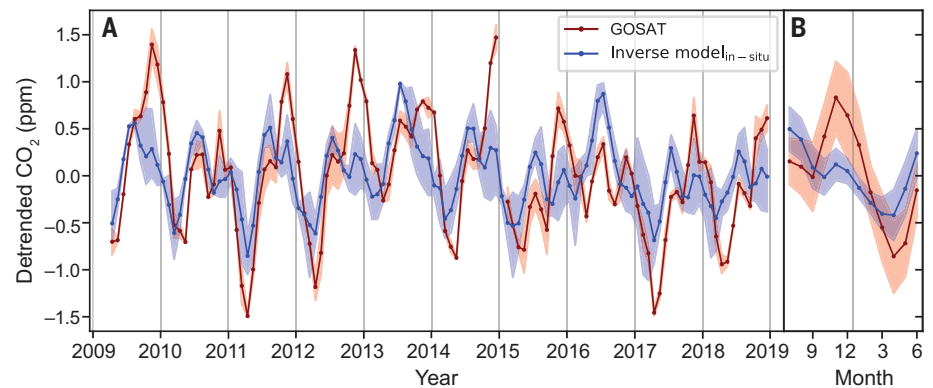

Fig. 1. Detrended CO_2 concentrations over Australia from satellite and models. (**A**) Detrended column-average dry-air mole fractions of CO_2 measured by GOSAT (red) and simulated by inverse models assimilating in situ ground-based measurements (blue). Data are monthly averages for Australia. Red shading indicates the range of the GOSAT/RemoTeC and GOSAT/ACOS algorithms. Blue shading indicates the range of the CarbonTracker, CAMS, and TM5-4DVAR inverse models. ppm, parts per million. (**B**) Mean and standard deviation (shading) over the period 2009–2018.
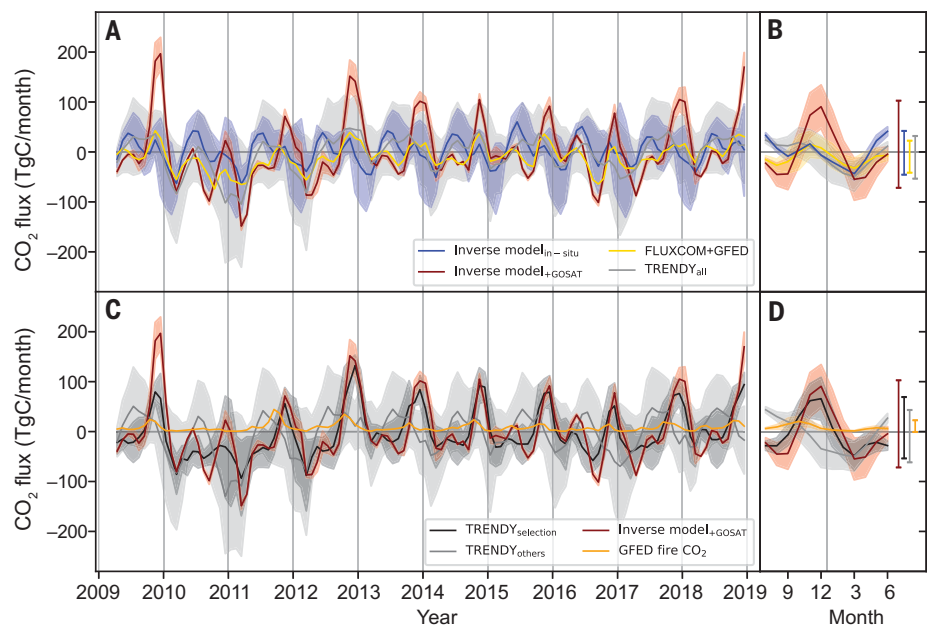

Fig. 2. Australian net CO_2 fluxes. (**A**) Top-down estimates of the net monthly Australian CO_2 fluxes inferred by in situ CO_2 measurement–based inverse models (blue) and by TM5-4DVAR assimilating in situ measurements together with GOSAT observations (red), compared with bottom-up FLUXCOM+GFED NBP (yellow) and the TRENDY ensemble mean NBP (gray). Shading indicates the range among the various top-down data streams (in situ–based CarbonTracker, CAMS, and TM5-4DVAR in blue, TM5-4DVAR+GOSAT/RemoTeC and TM5-4DVAR+GOSAT/ACOS in red) and the standard deviation among the TRENDY ensemble (gray). (**C**) NBP of a subgroup of TRENDY models (black) compared with the other models (gray), with the GOSAT inversions [red, same as in (A)], and with GFED fire emissions (orange). Shading as in (A). (**B** and **D**) Mean and standard deviation (shading) over the period 2009–2018 and the mean peak-to-peak seasonal cycle amplitudes (bars). Positive fluxes correspond to carbon emissions into the atmosphere.

pulses (Fig. 2A), and its seasonal amplitude (64 ± 16 TgC/month) underestimates the one found by the GOSAT inversions by a factor of three. This could be explained by the sparsity of Australian flux tower data in the training of the FLUXCOM machine learning models (only 4 of 224 sites are located in Australia; see fig.

S3), causing extrapolation errors (18), and by known weaknesses in representing certain fluctuations in response to water availability (19) or "memory" effects due to unaccounted carbon pool dynamics (43). Our analysis further suggests that local and transported fire emissions might contribute at the beginning of the

Fig. 3. Seasonal timing of gross CO$_2$ fluxes among TRENDY models. (**A**) Gross primary production (GPP, green) and total respiration (TER, purple) for Australia for the selection of TRENDY DGVMs that replicate the end-of-dry-season CO$_2$ pulses. The difference of TER and GPP is given in black in the lower part together with GOSAT-based inversion where GFED fire emissions are subtracted (dashed red line). (**B**) Same as (A), but for the other TRENDY models that do not replicate the end-of-dry-season CO$_2$ pulses. (**C**) Mean monthly precipitation over the entire Australian region (black) and the semiarid part (fig. S3) of Australia (blue).
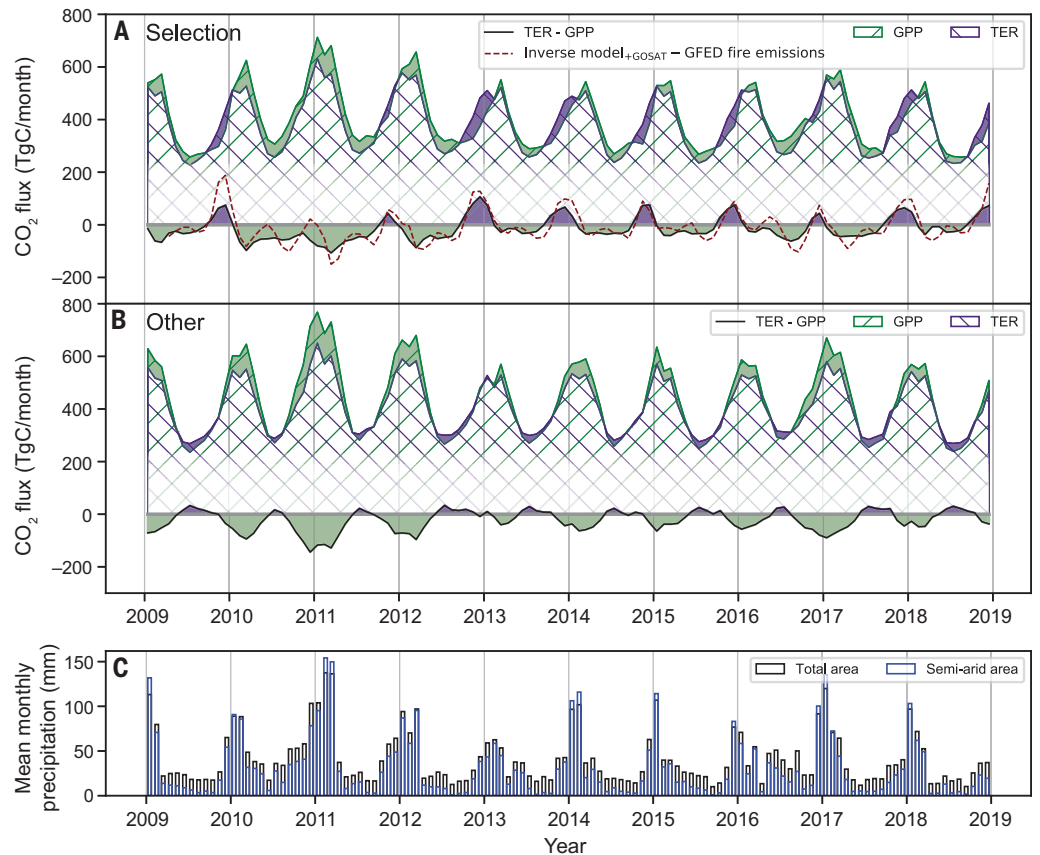
carbon pulses but cannot explain their magnitude and duration (Fig. 2B and fig. S8).

The ensemble of TRENDY NBP simulations shows a large intermodel spread and also no end-of-dry-season CO$_2$ pulses on average (Fig. 2A) causing a seasonal amplitude (85 ± 20 TgC/month) that is about half of that of the GOSAT inversions. However, the dry season pulses are present in a subset of five of the TRENDY DGVMs [Fig. 2B and table S1; "Characteristics of TRENDY$_{selection}$" in (34)]. For this subset, the timing, duration, and magnitude (except for the year 2009) of the pulses and their seasonal amplitude (123 ± 31 TgC/month) are closer to the pulses found by the GOSAT inversions. This finding suggests that the CO$_2$ pulses can be explained by ecosystem processes shaping the phasing of photosynthesis and respiration.

Phasing of respiration and photosynthesis

We find that the subset of DGVMs that are in good agreement with the GOSAT inversions reveal a distinctly different seasonal timing of GPP and TER than the other DGVMs. For the selected subset, the CO$_2$ pulses are driven by TER, which increases rapidly at the onset of the rainy season, whereas GPP picks up only a few weeks later (Fig. 3A). The pulses originate mainly from an early increase of soil respiration in semiarid regions (figs. S9 and S10A). For the other DGMVs, TER and GPP show a

mostly synchronous phasing throughout the year, yielding no CO$_2$ pulses (Fig. 3B and fig. S10B). The precipitation records for the semiarid regions of Australia (Fig. 3C and fig. S3) suggest that the soil respiration–driven pulses shown by the GOSAT inversions and the selected TRENDY models are weaker or do not occur in years with anomalously strong precipitation during the dry period (Austral winter), such as in the La Niña years 2010 and 2016. This implies that the observed pulses are conditional on rewetting of dry soils and that it is through the strength of the pulses that climatic conditions exert control over Australia's annual CO$_2$ balance (fig. S6).

The detected continental-scale CO$_2$ pulses are consistent with site-level observations of dryland ecosystems that show an asynchronous response of respiration and photosynthesis to precipitation pulses (44). The rapid response of microbial respiration to rewetting events is known as the "Birch effect" and has been described in the literature of specific sites in some semiarid regions for many decades (30–32). After being dormant in the dry period, soil microbes are activated by the moisture supply from rainfall. Under warm soil temperatures, the microbes quickly respire accumulated and readily available substrate and their populations grow rapidly. These dynamics of soil microbial processes cause respiration CO$_2$ pulses with

rewetting of dry soils that are evident in Australian flux tower data (figs. S11 and S12). Photodegradation of surface litter (45) and the death of microorganisms during the dry period (46, 47) may lead to the accumulation of easily decomposable substrate available to microorganisms at the onset of rain. It remains an open question whether the respiration pulses are mainly driven by substrates accumulated during the dry period and to what extent they are fueled by mobilization and decomposition of physically protected carbon (47). These processes are not represented explicitly or in detail in the TRENDY DGVMs, and thus the DGVMs cannot resolve how the site-level mechanisms scale up to the continental-scale effect observed here. Nonetheless, a selection of models effectively captures the continental-scale CO$_2$ pulses by a fast response of respiration and a delayed response of photosynthesis to the onset of the rainy season. This highlights the importance of subtle differences in effective parameterizations of respiration and photosynthesis to moisture fluctuations. Associated uncertainties affect the ability of the models to accurately represent the carbon cycle of semiarid ecosystems.

Our study demonstrates that the soil respiration–driven CO$_2$ pulses over Australia after the end of the dry season are of large-scale relevance and appear to dominate the variability of the continent's carbon balance.

The GOSAT inversions have shed light on a blind spot of previous top-down and bottom-up approaches for quantifying and attributing CO_2 flux variability. This is important because Australia's semiarid regions contribute substantially to the interannual variability of the global terrestrial carbon sink and because it is the ecosystem response to the phasing of dry and wet periods that drives the seasonal mechanism behind the large interannual variability. Thus, our study calls for revisiting the contributions of global semiarid systems to CO_2 balance variations and for assessing implications for our ability to model climate-carbon feedbacks in semiarid regions. Only a few of the global vegetation models are able to reproduce the observed CO_2 pulses, which suggests that only their respective parameterizations are able to represent the sensitivity of the underlying mechanism to changes in climatic conditions and, thus, to accurately project semiarid CO_2 flux variability under a changing climate. Considering the large uncertainties associated with modeling climate-carbon feedbacks (14, 15, 48), our findings may contribute continental-scale mechanistic understanding that can help reduce these uncertainties for dryland ecosystems that are found to be particularly sensitive to climate change (49).

REFERENCES AND NOTES

1. P. Friedlingstein et al., Earth Syst. Sci. Data 12, 3269–3340 (2020).
2. B. Poulter et al., Nature 509, 600–603 (2014).
3. A. Ahlström et al., Science 348, 895–899 (2015).
4. M. Jung et al., Nature 541, 516–520 (2017).
5. V. Humphrey et al., Nature 592, 65–69 (2021).
6. S. Piao et al., Glob. Change Biol. 26, 300–318 (2020).
7. V. Haverd, A. Ahlström, B. Smith, J. G. Canadell, Glob. Change Biol. 23, 793–800 (2017).
8. R. G. Detmers et al., Geophys. Res. Lett. 42, 8177–8184 (2015).
9. X. Ma et al., Sci. Rep. 6, 37447 (2016).
10. J. Cleverly et al., Sci. Rep. 6, 23113 (2016).
11. Z. Xie et al., Remote Sens. Environ. 231, 111270 (2019).
12. A. Bastos et al., Global Biogeochem. Cycles 34, e2019GB006393 (2020).
13. L. Teckentrup et al., Biogeosciences 18, 5639–5668 (2021).
14. P. M. Cox, C. Huntingford, M. S. Williamson, Nature 553, 319–322 (2018).
15. S. Wenzel, P. M. Cox, V. Eyring, P. Friedlingstein, Nature 538, 499–501 (2016).
16. D. L. Hoover, A. A. Pfennigwerth, M. C. Duniway, J. Ecol. 109, 3280–3294 (2021).
17. N. MacBean et al., Environ. Res. Lett. 16, 094023 (2021).
18. G. Tramontana et al., Biogeosciences 13, 4291–4313 (2016).
19. P. Bodesheim, M. Jung, F. Gans, M. D. Mahecha, M. Reichstein, Earth Syst. Sci. Data 10, 1327–1365 (2018).
20. M. Jung et al., Biogeosciences 17, 1343–1365 (2020).
21. S. Sippel et al., Curr. Clim. Change Rep. 4, 266–286 (2018).
22. J. Beringer et al., Biogeosciences 13, 5895–5916 (2016).
23. J. Cleverly et al., Environ. Res. Lett. 14, 095004 (2019).
24. P. J. Sellers, D. S. Schimel, B. Moore 3rd, J. Liu, A. Eldering, Proc. Natl. Acad. Sci. U.S.A. 115, 7860–7868 (2018).
25. P. I. Palmer et al., Nat. Commun. 10, 3344 (2019).
26. B. Byrne et al., J. Geophys. Res. Atmos. 125, e2019JD032029 (2020).
27. Z. Chen et al., Environ. Res. Lett. 16, 054041 (2021).
28. Y. Villalobos, P. Rayner, S. Thomas, J. Silver, Atmos. Chem. Phys. 20, 8473–8500 (2020).
29. S. Sitch et al., Biogeosciences 12, 653–679 (2015).
30. H. F. Birch, Plant Soil 20, 43–49 (1964).
31. P. Jarvis et al., Tree Physiol. 27, 929–940 (2007).
32. P. Casals, L. Lopez-Sangil, A. Carrara, C. Gimeno, S. Nogués, Global Biogeochem. Cycles 25, GB3012 (2011).
33. A. Kuze et al., Atmos. Meas. Tech. 9, 2445–2461 (2016).
34. Materials and methods are available as supplementary materials.
35. A. Butz et al., Geophys. Res. Lett. 38, L14812 (2011).
36. T. E. Taylor et al., Earth Syst. Sci. Data 14, 325–360 (2022).
37. A. Eldering et al., Science 358, eaam5745 (2017).
38. Y. Villalobos et al., Atmos. Chem. Phys. Discuss. 22, 8897–8934 (2022).
39. D. Wunch et al., Philos. Trans. R. Soc. London Ser. A 369, 2087–2112 (2011).
40. W. Peters et al., Proc. Natl. Acad. Sci. U.S.A. 104, 18925–18930 (2007).
41. F. Chevallier et al., J. Geophys. Res. 115, D21307 (2010).
42. S. Basu et al., Atmos. Chem. Phys. 13, 8695–8717 (2013).
43. S. Besnard et al., PLOS ONE 14, e0211510 (2019).
44. T. E. Huxman et al., Oecologia 141, 254–268 (2004).
45. F. E. Moyano, S. Manzoni, C. Chenu, Soil Biol. Biochem. 59, 72–85 (2013).
46. W. Borken, E. Matzner, Glob. Change Biol. 15, 808–824 (2009).
47. J. P. Schimel, Annu. Rev. Ecol. Evol. Syst. 49, 409–432 (2018).
48. V. K. Arora et al., Biogeosciences 17, 4173–4222 (2020).
49. X. Lian et al., Nat. Rev. Earth Environ. 2, 232–250 (2021).
50. A. Butz, RemoTeC full-physics retrieval GOSAT/TANSO-FTS Level 2 bias-corrected XCO2 version 2.4.0 operated at Heidelberg University, RemoTeCv2.4.0, Zenodo (2022); https://doi.org/10.5281/zenodo.5886662.
51. E.-M. Metz, ATMO-IUP-UHEI/MetzEtAl2023: v1.0.0, version 1.0.0, Zenodo (2023); https://doi.org/10.5281/zenodo.7648699.

SUPPLEMENTARY MATERIALS

Soil respiration–driven CO$_2$ pulses dominate Australia's flux variability

Eva-Marie Metz, Sanam N. Vardag, Sourish Basu, Martin Jung, Bernhard Ahrens, Tarek El-Madany, Stephen Sitch, Vivek K. Arora, Peter R. Briggs, Pierre Friedlingstein, Daniel S. Goll, Atul K. Jain, Etsushi Kato, Danica Lombardozzi, Julia E. M. S. Nabel, Benjamin Poulter, Roland Sfrian, Hanqin Tian, Andrew Wiltshire, Wenping Yuan, Xu Yue, Snke Zaehle, Nicholas M. Deutscher, David W. T. Griffith, and Andr Butz

The exhalation of drylands

Semi-arid regions cause much of the interannual variability in global atmospheric carbon dioxide concentration because of seasonal fluctuations in water availability. Metz *et al.* found that recurrent carbon dioxide pulses occur at the end of the dry season over Australia, an effect that they attribute to enhanced soil respiration preceding photosynthetic uptake in semi-arid regions. The magnitudes of these pulses are two to three times larger than previous studies have inferred based on in situ measurements. —HJS

View the article online
https://www.science.org/doi/10.1126/science.add7833
Permissions
https://www.science.org/help/reprints-and-permissions

Use of this article is subject to the Terms of service